

# Patient-specific prediction of regional lung mechanics in ARDS patients with physics-based models: A validation study

Maximilian Rixner<sup>1\*</sup>, Maximilian Ludwig<sup>2</sup>, Matthias Lindner<sup>3</sup>, Inéz Frerichs<sup>3</sup>, Armin Sablewski<sup>3</sup>, Karl-Robert Wichmann<sup>1</sup>, Max-Carl Wachter<sup>1</sup>, Kei W. Müller<sup>1</sup>, Dirk Schädler<sup>3</sup>, Wolfgang A. Wall<sup>1,2</sup>, Jonas Biehler<sup>1†</sup>, Tobias Becher<sup>3†</sup>

<sup>1</sup>Ebenbuild GmbH, Munich, Germany.

<sup>2</sup>Institute for Computational Mechanics, Department of Engineering Physics and Computation, TUM School of Engineering and Design, Technical University of Munich, Germany.

<sup>3</sup>Department of Anesthesiology and Intensive Care Medicine, University Medical Center Schleswig-Holstein Campus Kiel, Germany.

\*Corresponding author(s). E-mail(s): [rixner@ebenbuild.com](mailto:rixner@ebenbuild.com);

†These authors contributed equally to this work, shared last authorship.

## Abstract

**Background:** The choice of lung protective ventilation settings has a considerable impact on patient outcomes, yet identifying optimal ventilatory settings for individual patients remains highly challenging. This is due to the high inter- and intra-patient anatomical and pathophysiological variability associated with ARDS in particular. In this study, we demonstrate that physics-based computational lung models tailored to individual patients can resolve this variability, predicting the otherwise unknown local states of the pathologically affected lung and thereby enabling a quantitative analysis of regional ventilation and mechanical load exerted on parenchymal tissue during mechanical ventilation.

**Methods:** For seven ARDS patients undergoing invasive mechanical ventilation, physics-based, patient-specific lung models was created based on chest CT scan and ventilatory data. By numerically resolving the interaction of the pathological lung with the airway pressure and flow imparted by the ventilator, we predict the time-dependent and heterogeneous local state of the lung and its regional ventilation for each patient. The model-predicted regional ventilation is then assessed and quantitatively compared with the regional ventilation obtained from bedside monitoring by Electrical Impedance Tomography.

**Results:** The predictions of the regional ventilation by the computational lung models showed excellent agreement with the EIT findings. The model-predicted anteroposterior ventilation profile achieved a Pearson correlation of 96% with the clinical reference data. Even when considering the regional ventilation within the entire transverse chest cross-section and across the entire dynamic ventilation range, an average correlation of more than 81% and an average root mean square error of less than 15% were achieved.

**Conclusion:** The results of this first systematic validation study show that our computational lung models accurately predict regional ventilation phenomena within the lung. The findings thereby demonstrate that our patient-specific models can provide clinically relevant information, which could enable a truly patient-specific choice of ventilator settings based on both individual anatomy and pathophysiology.

**Keywords:** ARDS, Patient-Specific Models, Mechanical Ventilation, Electrical Impedance Tomography

# 1 Background

While mechanical ventilation often constitutes the only viable treatment for patients suffering from hypoxemic respiratory failure, it also poses an inherent dilemma. Subjecting the lung parenchyma to mechanical ventilation in itself can lead to further ventilator-induced lung injury (VILI) [1, 2]. VILI is caused by several mechanisms and pathways, such as volutrauma and barotrauma due to excessive strain and stress, or atelectrauma due to repeated alveolar collapse and re-opening [3–5]. Common to these mechanisms is that they are hard to detect clinically and pertain to heterogeneity and spatial variability on relatively small length scales. Consolidations and atelectasis act as local stress risers [6], which are inaccessible to direct imaging or measurements. While the fundamental causality of VILI is primarily a mechanical phenomenon, it is also intricately linked to biochemical processes at the microscopic level, such as the exacerbation of inflammatory responses [7]. Recognizing VILI as a major factor contributing to high mortality and morbidity has significantly advanced acute respiratory distress syndrome (ARDS) treatment [8]. It is now widely accepted that lung-protective mechanical ventilation must minimize cumulative biotrauma while simultaneously ensuring adequate gas exchange and hemodynamic stability.

In juxtaposition to the general agreement regarding the necessity of lung protective ventilation lies the lack of any clear consensus on the *specific* optimal ventilation strategy for an individual patient. This holds particularly true in the case of ARDS, which, as a complex and clinically heterogeneous syndrome, is inherently challenging to treat, involving different phenotypes and comorbidities. Current standard-of-care still largely relies on broad population-average heuristics [9] with relatively simple criteria, such as an acceptable range of tidal volume as a function of predicted body weight (4-8 mL/kg) [10, 11]. This approach, however, fails to account for inter- and intra-patient variability [12] and the unresolved heterogeneous pathologies and mechanical properties of the lung tissue lead to patient-specific responses and heterogeneity of treatment effects [13, 14]. This is in line with recent clinical studies on optimal mechanical ventilation strategies for ARDS increasingly encountering inconsistent and inconclusive results as a consequence of the unresolved heterogeneity and complex pathophysiology [15] and - unfortunately - also in line with the observation that patient outcome for ARDS has stagnated for more than two decades. Mortality remains high at roughly 40% [16, 17].

The inability to further advance patient outcome employing general treatment protocols has led to attempts to inform ventilation strategies based on additional patient-specific information (e.g., EIT

[18]), attempts to stratify the inherent variability of ARDS into further latent subgroups and phenotypes [19–22], as well as general calls for the development of new, precision-guided medical approaches for lung protective ventilation [23, 24].

Researchers have also proposed the use of data-driven reinforcement learning [25, 26] for the identification of optimal ventilatory settings. In essence, this approach mimics a highly experienced physician by looking at past treatment trajectories in order to identify optimal choices, leveraging the excellent ability of machine learning algorithms to discern patterns in large corpi of historical clinical data. Beside lacking interpretability and explainability, it is also limited both to historical data as well as global descriptions of the patient and the lung. The lung itself continues to remain a black box to the treating clinician, and regional lung mechanics and heterogeneous ventilation - key factors underlying VILI - are not taken into account.

In our opinion, providing truly patient-specific lung protective ventilation requires to move beyond the lung as a black box, considering the complex interactions of pressure and airflow within the lung parenchyma while accounting for the individual pathophysiology and heterogeneity. We believe that patient-specific, physics-based computational lung models present the most promising way to provide physicians with detailed, quantitative information about individual pathophysiology and regional lung mechanics. Predictive models do not only enable a detailed analysis of the current state of the lungs but also the evaluation of hypothetical scenarios to determine the optimal treatment for a patient without having to test different settings directly on the patient.

While several computational lung models have been developed in the past [27–29], many models lack the spatial resolution to resolve the heterogeneity within the lung [30–33]. The results presented here are based on our development of a reduced dimensional lung model, [34–37], which has the unique ability to reflect patient-specific anatomy, pathophysiology, and still provides results within clinically relevant time frames. A prerequisite for their clinical application is the demonstration of their predictive capability and accuracy regarding regional ventilation and strain against measured data, which is the purpose of this study.

## 2 Material and Methods

Building upon and extending previous work [27, 35], this validation study assesses the accuracy of patient-specific lung models for a cohort of patients suffering from ARDS and undergoing invasive mechanical ventilation. In order to construct and calibrate models which are able to resolve the underlying physics with a high degree of fidelity, we make use of a routine clinical chest computed

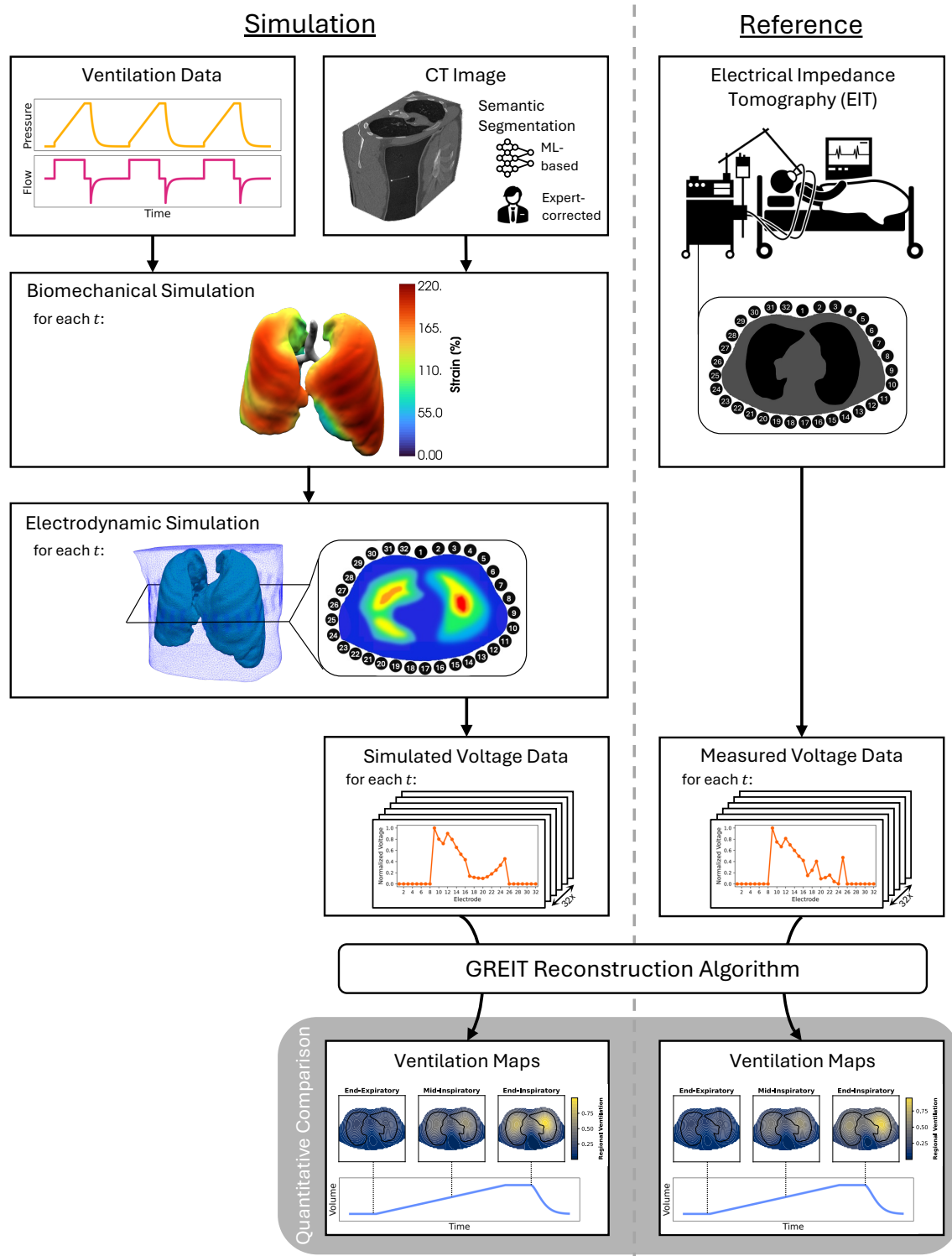


**Fig. 1:** Conceptual overview - validation of computational lung model against clinical reference data. *Reference:* Using an electrode belt positioned around the thorax of the patient, we can observe the regional ventilation during mechanical ventilation (EIT). *Simulation:* On the basis of a computed tomography (CT) scan we construct a patient-specific model of the lung and conduct a biomechanical and electrodynamic simulation, mimicking both the mechanical ventilation process and the propagation of electrical currents across the patient's torso. The simulated voltages obtained from the computational lung model yield a *virtual* EIT, which we compare against the bedside EIT obtained from clinical, measured voltage data for a series of timesteps  $t$ .

tomography (CT) as well as data exported from the mechanical ventilator. Afterwards, the computational lung model is used to simulate the process of mechanical ventilation and yields predictions of regional mechanical quantities such as ventilation distribution and strain subject to intra- and inter-patient variability. We validate these predictions by comparing them against the regional ventilation distribution obtained from bedside Electrical Impedance Tomography (EIT).

This entire process underlying the model validation is summarized in Figure 1. The right side shows the process of obtaining bedside measured EIT electrode voltage data, and subsequently reconstructing the regional ventilation distribution from them, i.e., obtaining EIT images. EIT produces a dynamic low-resolution image that corresponds to regional changes in electrical bioimpedance of lung tissue and, thereby, visualize the amount of regionally contained air against a predefined baseline, usually at end-expiration. We emphasize that the measured voltage data from EIT is not used for model generation or calibration, but exclusively serves as the reference against which we compare the model-predicted regional ventilation. Correspondingly, the entire process of obtaining model-predicted regional ventilation is outlined on the left-hand side of Figure 1. As a first step, the patient-specific biomechanical model of the respiratory system - further described in the subsequent sections - is constructed for each study participant using a chest CT and ventilatory data, enabling the personalized prediction of the time-dependent global and local state of the lung parenchyma during mechanical ventilation. Our model can predict, among other quantities, regional strain and ventilation state. The results of the biomechanical simulation enables us to inform a subsequent electrodynamic simulation, computing the propagation of electromagnetic fields across the patient’s torso as a function of the model-predicted regional ventilation state. We apply the same electrical stimuli in the electrodynamic simulation as the EIT device in the patient, thereby obtaining *simulated* voltage data.

The reconstruction of the ventilation distribution from either simulated or measured voltage data is possible due to the dependence of the conductivity of the lung parenchyma on the *local* aeration. Hence, utilizing the electrode voltage data, we can ascertain regional ventilation through the application of an appropriate reconstruction algorithm. After obtaining the model-predicted and reference ventilation distribution based on model-predicted and measured voltage data, respectively, a quantitative comparison is conducted, to validate the models predictions.

The electrodynamic simulation and subsequent reconstruction of regional ventilation might seem superfluous at first glance; however, by incorporating the electrodynamic simulation and ensuring that

the regional ventilation follows from the *identical* sequence of steps - including physical characteristics and reconstruction-specific influences underlying EIT - we ensure the *consistent* comparison of the regional ventilation arising from both model predictions and measured reference data.

## 2.1 Clinical Data

For this study, we analyzed data that was collected within the scope of the SMART-Study (DRKS-ID: DRKS00017151). The primary purpose of this study was to validate computational models that predict not just strain but also recruitment/de-recruitment processes during recruitment maneuvers or decremental PEEP trials, which is not within the scope of this work. A publication describing the entirety of the clinical dataset, as well as study and project results, is forthcoming. Here, we only describe a subset of the data as relevant to our work in a dual-use setting, comprising various data throughout regular pressure-controlled ventilation at fixed ventilation settings. Briefly, ARDS patients were eligible for study inclusion if (i) they met the Berlin definition [38], (ii) required mechanical ventilation and (iii) a thoracic CT scan was carried out within 24 hours before their study enrolment. Exclusion criteria were age less than 18 years, pregnancy, presence of a cardiac pacemaker or other implantable electronic devices, higher-grade burns, or skin lesions in the area of the EIT belt placement, high-grade chronic obstructive lung disease, and hemodynamic instability despite adequate fluid and catecholamine therapy. The study was approved by the Ethics Committee of the Medical Faculty of the Christian-Albrechts-Universität Kiel and carried out in accordance with the Helsinki Declaration. Written informed consent was obtained from all patients or their legal representatives.

CT images were acquired with a Siemens Somatom or Philips IQon scanner at a pre-defined pressure state corresponding to end-expiratory lung volume with an in plane resolution of 512x512 and a slice thickness of 2 mm according to routine clinical practice at the University Medical Center in Kiel. For all patients, EIT examinations were carried out using the Elisa 800 (Löwenstein Medical, Bad Ems, Germany) with the textile 32-electrode belt placed around the patient’s chest circumference in one slightly oblique transverse plane at the level of the 4th or 5th intercostal space, measured in the parasternal line. Figure 2 shows exemplary slices of the chest CT at the height where the EIT belt was placed. Moreover, the shown slices highlight the regional heterogeneity of the lungs with bilateral infiltrates and pulmonary edema. In addition to the CT and EIT data, we used airway pressure, air flow, and esophageal pressure recorded during 10 breathing cycles of pressure-controlled ventilation.

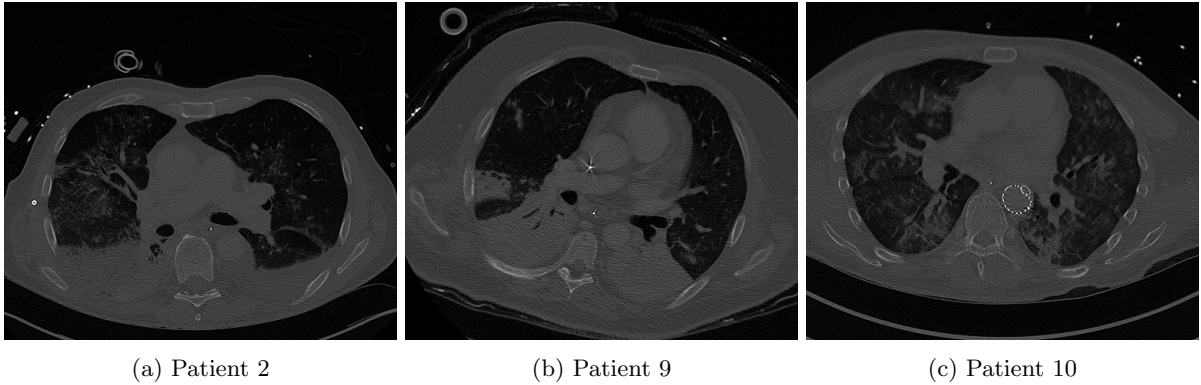


**Fig. 2:** Exemplary transverse CT slices at the level of the EIT belt between 4<sup>th</sup> or 5<sup>th</sup> intercostal space defining the EIT reconstruction plane acquired in three of the studied patients.

## 2.2 Computational Lung Model

For each study participant, we created a patient-specific computational model capable of predicting airflow and tissue distention as well as their interaction throughout the respiratory system. To achieve this, we first extract pertinent structures of the respiratory system from a chest CT using computer vision and deep learning, obtaining a patient-specific anatomic representation of the lungs, lobes, and airways.<sup>1</sup> Following this approach as depicted in Figure 3, the patient-specific physiological features are then subsequently translated to reduced-dimensional computational elements representing the behavior of airways and the lung parenchyma, with volumetric and constitutive effects of the lung parenchyma being locally informed on the basis of Hounsfield attenuation values [34, 35, 39]. Insights into typical constitutive behavior of lung tissue have been gained via extensive experimental studies on living lung tissue samples [40–43]. In addition to the CT, respiratory time series data from the mechanical ventilator is used to calibrate and inform global respiratory system characteristics of the model. Since the computational model is derived from *first principle*, i.e., it is based on the description of fundamental physical laws, it allows extrapolative prediction of *regional* lung mechanics and its interaction with forcing airflow and pressure (see exemplarily the strain field depicted in Figure 3). We refer the interested reader to the supplementary materials (Appendix A) for a more detailed description of the reduced dimensional computational lung model and its calibration, as well as to aforementioned prior work [34, 35, 39] for full mathematical details. To ensure reproducibility and scalability, the entire model generation process has been automated by implementing it as in-house software packages and integrating it within an end-to-end computing pipeline.

<sup>1</sup>Since this study focuses on the validation of the physics-based computational model, additional manual inspection and correction of the segmentation masks was carried out to ensure absolute correctness.

The resulting patient-specific, physics-based simulation models account for individual anatomy as well as pathophysiology. In particular, the model captures the elastic interaction of the lungs with the rib cage and diaphragm and accounts for the hydrostatic pressure resulting from gravitational load and patient positioning. As a result, we can predict - among others - regionally resolved transient airflow, ventilation, strain, and stress over the entire lung for arbitrary - real or hypothetical - ventilation settings. The only required input for the computational model is the sequence of pressure or flow values enforced by the ventilator at the endotracheal tube and patient positioning. Exemplary model predictions, showing how the regional strain of the lung parenchyma changes with different pressure levels applied by the mechanical ventilator, are shown in Figure 4.

## 2.3 Electrodynamic Simulation

On the basis of the bedside EIT carried out for each study participant, we used the measured voltage data - resulting from electrical stimulations and measurements around the chest - to reconstruct the regional ventilation distribution of the lung during mechanical ventilation. This reconstructed time-dependent regional ventilation serves as the ground truth and will be quantitatively compared against the regional ventilation predicted by the computational lung model. To ensure a *consistent* representation of the regional ventilation, the biomechanical model is used to inform the temporal and spatial variability of the conductivity of the lung parenchyma during mechanical ventilation [44], enabling an electrodynamic simulation to resolve the propagation of electrical currents across the thorax. By precisely mirroring the stimulation patterns and placement of electrodes employed during bedside EIT, we obtain *simulated* voltage data in complete equivalence to the measured clinical voltage data (Figure 1). Subsequently applying the identical reconstruction algorithm to the simulated voltage data yields a model-derived *virtual* EIT,

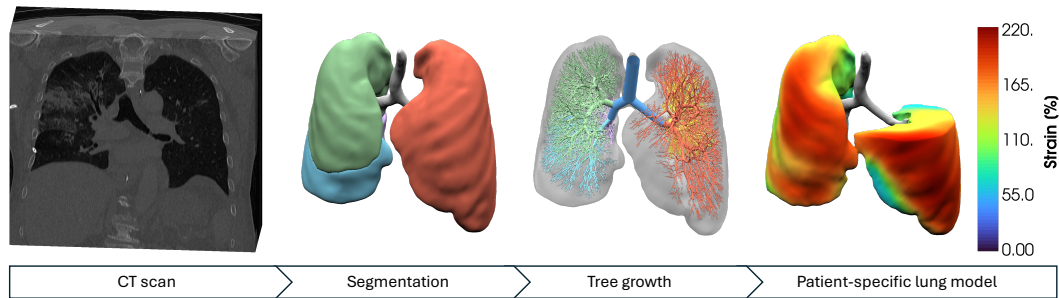


**Fig. 3:** With a high-resolution CT scan as input, the generation of patient-specific models is a streamlined process starting with the segmentation of the voxel data into airways, lungs, and lobes. Beyond the resolution limitations of the CT, a morphology-based tree growth algorithm creates the remaining generations of conducting airways in a space-filling manner (for a total of 16 generations). Finally, a patient-specific computational lung model is constructed to predict regional lung mechanics, such as the strain or regional ventilation of the lung parenchyma during mechanical ventilation.

which is directly comparable to the clinical bedside EIT.

This indirect approach is chosen because the physical phenomena and reconstruction algorithm underlying EIT generally impact the inferred regional ventilation distribution. By not just simulating the biomechanical processes within the lung during mechanical ventilation but additionally also the precise mechanism by which the regional ventilation has been inferred *in vivo*, we ensure consistency and comparability between model predictions and clinical measurements.

Reconstruction of regional ventilation from the measured or simulated voltage measurements is performed using GREIT (*Graz consensus Reconstruction algorithm for EIT*) [45] both because it is as close as possible to an established standard, and also because an implementation is readily available within the open source framework EIDORS [46]. Our corresponding source code for the electrodynamic simulation and the EIT reconstruction on the basis of EIDORS is available online<sup>2</sup>. Further technical details concerning EIT and the reconstruction algorithm are provided in the supplementary materials (Appendix A).

### 3 Results

Overall, 10 patients were enrolled in the study. For this work, one patient had to be excluded from the analysis due to loss of EIT data. Two additional patients had to be excluded because undue noise within the recorded voltage data prevented obtaining any physiological and stable reconstructions of the regional ventilation. Thus, we conducted the assessment of the predictive capabilities of our model for 7 patients.

As a reminder, in the following we will assess and quantify the agreement of the regional ventilation as predicted by the model (simulation), comparing

<sup>2</sup><https://gitlab.com/xenotaph3/holoshed>

it against the bedside EIT (reference). In our notation we will consistently use (*s*) and (*r*) to delineate between quantities arising from (s)imulation and (r)eference clinical data, respectively. Following this convention, we denote the voltage data from clinical reference measurement as  $v^r(t)$  and the voltage data from biomechanical and electrodynamic simulation as  $v^s(t)$ . Using GREIT as a reconstruction algorithm, both simulated as well as measured voltage data are mapped to their corresponding regional ventilation distribution, denoted as  $Z^s(t)$  and  $Z^r(t)$ . The regional ventilation distributions encoded by  $Z$  are recovered by the reconstruction algorithm and simply correspond to EIT images, i.e., a grid of pixel values with varying intensities corresponding to the reconstructed inverse conductivity change of the lung parenchyma.

If the computational model correctly resolves the regional phenomena within the lung parenchyma as a function of the pressure-controlled ventilation, the simulated EIT  $Z^s(t)$  should provide similar information regarding the *regional ventilation* state of the lung as the bedside EIT  $Z^r(t)$  acting as our reference.

At this point, it is important to note that identical results regarding regional ventilation would generally not be expected even without any model error. Discrepancies are inevitable, arising primarily from the unavoidable noise and epistemic uncertainty underlying the recorded clinical data, e.g., movement of attached electrodes, improper electrode contact, cardiac activity, or deviations of the lung from the assumed reference state. Additionally, the inverse problem underlying the EIT reconstruction is inherently ill-conditioned [47], imposing intrinsic bounds on the accuracy of EIT.

### Preprocessing

The measured voltage data  $v^r$  obtained from bedside EIT has been recorded at a temporal resolution of 50 Hz, and was passed through a low-pass filter with a cutoff frequency of 1.4 Hz to remove spurious

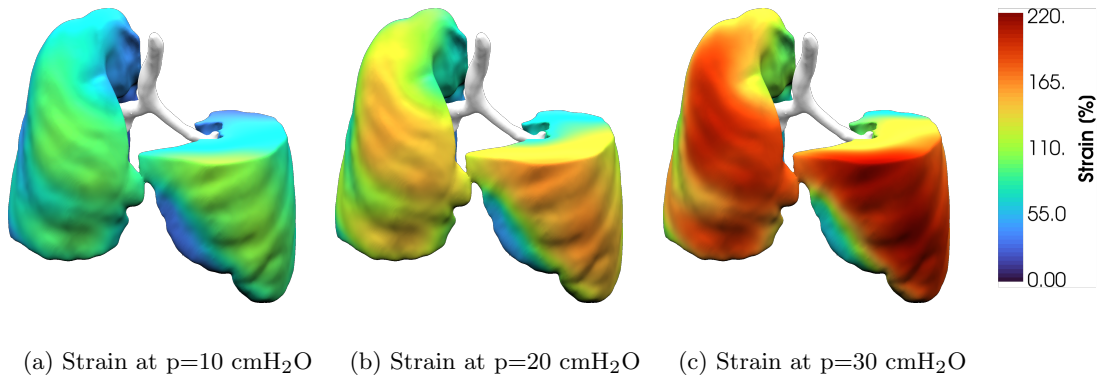


**Fig. 4:** Strain predictions for patient 2 during pressure-controlled ventilation at different points in time, showcasing the heterogeneous strain distribution within the lungs.

noise. As a further preprocessing step, EIT reconstructions resulting from GREIT were normalized to the unit range  $[0, 1]$  and subsequently clipped to the lung masks, as the objective is to assess the accuracy of the predicted regional ventilation *within* the lungs. This clipping operation to the lung masks is clearly evident in Figure 7, only showing *pulmonary pixels* within the lung masks.

### Data and Maneuver selection

To mitigate the confounding impact of measurement noise on results, all ensuing comparisons are based on a continuous time window  $t \in [t_1, t_2]$  comprising 10 identical pressure-controlled ventilation cycles. Time windows span approximately 30 seconds, and additionally contain a prolonged end-expiratory hold to establish a well-defined reference state required for difference EIT. Exemplary ven-

tilatory data associated with such a selected time is shown in Figure 5, showing both the measured data and model predictions. Since the tidal volume remained fixed across all 10 ventilation cycles, the lung repeatedly attains an identical ventilation state corresponding to a specific fraction of maximum observed end-inspiratory lung volume. By averaging over multiple time instances corresponding to the same inflation state, we obtain a more robust identification of the regional ventilation with reduced impact of measurement noise and cardiac activity.

### Quantitative Comparison

We divide our discussion of validation results into three subsections, successively expanding upon the spatial and temporal resolution of the comparison between model-predicted and clinically measured regional ventilation in each step. First, we assess model agreement at the end-inspiratory state based on regions of interest defined by the projection of the two-dimensional ventilation distribution onto the anteroposterior and the lateral axis, respectively. We chose this particular comparison because it has been previously employed in the validation of EIT against 4D-CT data [48] and as such the known agreement between EIT and 4D-CT data essentially provides us with an upper limit or benchmark for the achievable agreement between EIT and model predictions. In a second step, we directly compare ventilation distribution obtained from model predictions and measured voltage data at the end-inspiratory state at full available resolution of the EIT reconstructions, i.e., a pixel-wise comparison. We note that for practical reasons, the end-inspiratory state has been defined as having reached 95% of the tidal volume, i.e.,  $I(t) = 0.95$ , with  $I$  defined by the normalized cumulative sum of pixel intensities. Lastly, we investigate the agreement between model predictions and EIT measurements across the entire breathing cycle to demonstrate that our model can also capture the dynamic behavior of the lung across the full tidal range. To quantify the agreement of the regional ventilation

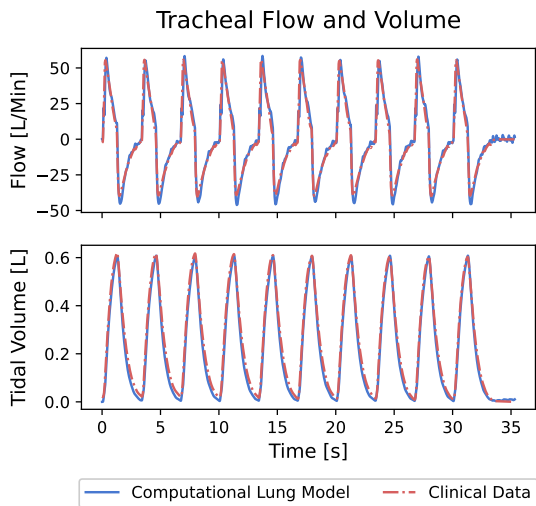


**Fig. 5:** Illustration of one exemplarily time-window underlying the validation, comprising 10 respiratory cycles. We compare the recorded flow rates and resulting tidal volumes exported from the mechanical ventilator (measured, clinical data) against the predictions obtained from the computational model. The waveforms are nearly identical.

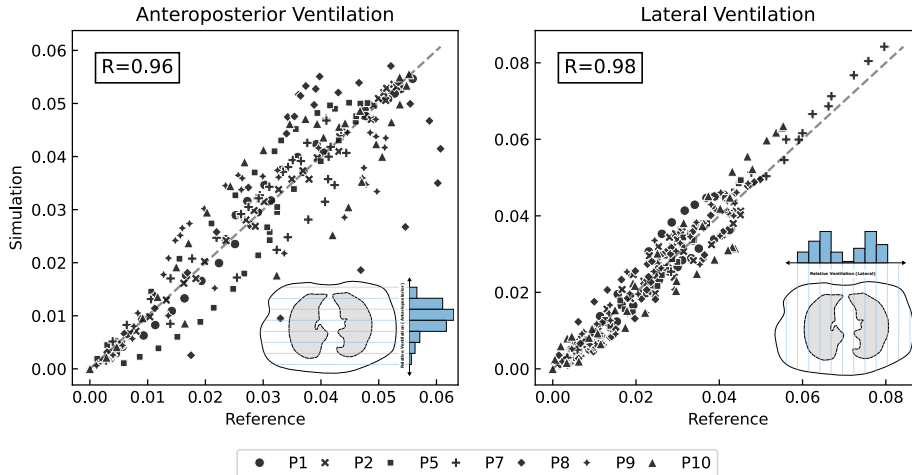


**Fig. 6:** The two-dimensional end-inspiratory ventilation map is projected (i) anterior to posterior and (ii) laterally left to right, yielding a Pearson correlation of  $R=0.96$  and  $R=0.98$ , respectively. The dashed line indicates the ideal unbiased one-to-one relationship of relative ventilation.

derived from model predictions and point-of-care pulmonary lung monitoring in the ICU, we will primarily report the linear Pearson correlation  $R$  and the root mean square error (RMSE) for all comparisons.

### 3.1 Regional Comparison at End-Inspiratory State

Validation results of pulmonary EIT - for instance against 4D-CT data — generally further simplify the description of the ventilation distribution using reduced descriptions such as, e.g., quadrants, center of ventilation, or anteroposterior ventilation distribution [49]. The reason for this approach is that achieving and demonstrating the accuracy of the full regional ventilation distribution within the context of the inverse problem implied by EIT is not a trivial undertaking, resulting from the previously mentioned challenges and limitations arising for both the reconstruction as well as data collection. As an initial step, we follow this approach and collapse the regional ventilation distribution to reduced descriptions, demonstrating similarity between computational lung model and measured clinical reference data on the basis of metrics already established in the relevant EIT validation literature. In particular we follow [48, 50] and project the regional ventilation distributions  $Z$  onto the one-dimensional axis that spans anterior to posterior, as well as additionally - for the sake of completeness - laterally. In contrast to other possible choices, such as the center of ventilation or quadrants, this has the benefit of maintaining a relatively high degree of spatial resolution, albeit decoupled across dimensions. Pooling the ensemble of seven patients and considering the local aerations along the two axes implied by the regional projections in Figure 6, we observe excellent agreement between computational model prediction and reference. In addition to the

very high degree of correlation of  $R = 0.96$  and  $R = 0.98$  for anteroposterior and lateral projections, respectively, we also note that the model predictions exhibit largely unbiased behavior. When this approach was applied to the validation of EIT itself against 4D-CT data in [48], the best result achieved was  $R = 0.89$  for the anteroposterior ventilation correlation. This implies that the model agreement with the measured clinical data is within proximity of the resolution limitations of EIT itself.

### 3.2 Comparison of End-Inspiratory Ventilation Distribution

In this section, we assess the agreement of the regional ventilation distribution for the *full* spatial resolution of EIT (across a transverse plane), thereby expanding beyond the resolution limitation of the regions of interest in the previous section. To this end, we obtain ventilation distributions using GREIT from simulated and measured voltage data at the end-inspiratory state at a resolution of  $64 \times 64$  pixels. The obtained reconstructions for the entire cohort are shown in Figure 7, with the top row illustrating the predicted ventilation distribution defined by the computational model and the bottom row showcasing the ventilation distribution obtained from the measured clinical voltage data. Summarizing the results, Table 1 presents the correlation  $R$  and RMSE of pulmonary pixel intensity values in arbitrary units (AU). On average, we observe a correlation of  $R = 0.82$  and a (normalized) RMSE = 0.14.

Note that the RMSE, due to the mentioned normalization of EIT reconstructions to the unit range, attains an interpretable nature as the percentage of deviation, with the discrepancy between model-predicted and clinical reference ranging from 10 to 20%. Together with visual inspection of the regional ventilation distributions depicted in Figure 7, which

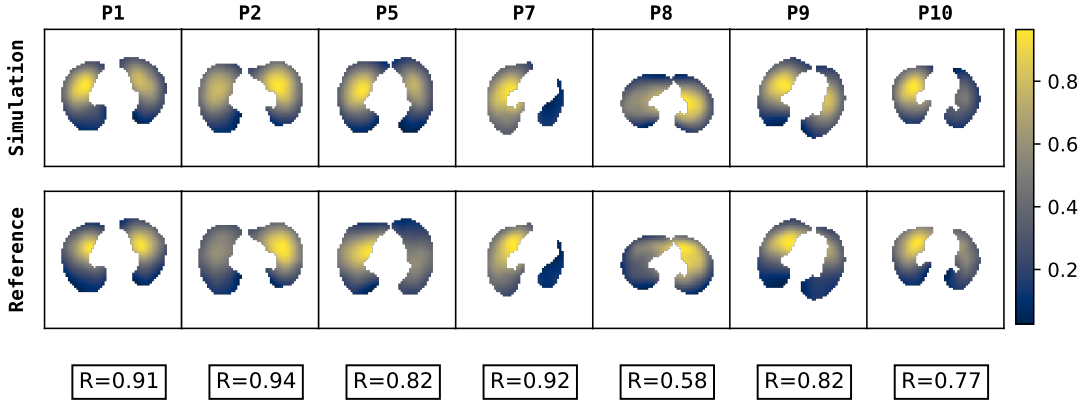


**Fig. 7:** Regional ventilation at the end-inspiratory state for each of the seven patients. Predictions of the computational model (top row) are compared against clinical reference data (bottom row), indicating also the correlation coefficient  $R$ . The EIT images are clipped to within the patient-specific lung masks known from the CT (i.e., pulmonary pixels).

Patient	1	2	5	7	8	9	10
R	0.91	0.94	0.82	0.92	0.58	0.82	0.77
RMSE	0.10	0.10	0.14	0.12	0.20	0.16	0.16

**Table 1:** Metrics reported for the validation cohort at end-inspiratory state.

for a subset of the patients approach visual indistinguishability, results demonstrate very good qualitative and quantitative agreement between model predictions and clinical reference data.

### 3.3 Comparison of Ventilation Distribution Across Full Tidal Range

The preceding discussion focused on assessing the accuracy of the model-predicted regional ventilation at the end-inspiratory state ( $I = 0.95$ ), at which the lung parenchyma experiences maximum inflation. To additionally study the dynamic model behavior, here we expand the previous discussion to the full tidal range occurring during ventilation. Since in such a setting we wish to disambiguate between regional distribution and global volume changes, we decompose both the model-predicted as well as reference ventilation distributions into the total amount of aeration present within the lung  $A(t)$ , as well as its normalized regional ventilation  $\hat{Z}(t)$ , i.e.,  $Z(t) = A(t) \cdot \hat{Z}(t)$ . By enforcing that  $\hat{Z}$  has a unit-norm it represents the regional ventilation distribution, while  $A(t)$  becomes a function of overall pulmonary pixel intensities, corresponding to the total amount of aeration present. On the basis of this representation we can then decompose the task of validation into (i) quantifying agreement of model-predicted and reference amplitudes  $A$  (total amount of aeration), as well as (ii) repeating our previous analysis of the regional distribution

from section (3.2) for  $\hat{Z}$  arising across multiple inflation states. For the ventilation amplitude  $A(t)$  as a scalar quantity it is straightforward to proceed, with Figure 8 illustrating the model’s ability to provide an accurate and unbiased prediction of the total amount of aeration of the lung (evaluated for a discrete set of inflation states). While we already expected the model to correctly resolve the total amount of aeration given its relatively straightforward *global* characteristic, the agreement evident in Figure 8 also demonstrates that the measured voltage data, additional electrodynamic simulation, and subsequent reconstruction using GREIT all behave as expected without introducing any notable distortion or bias.

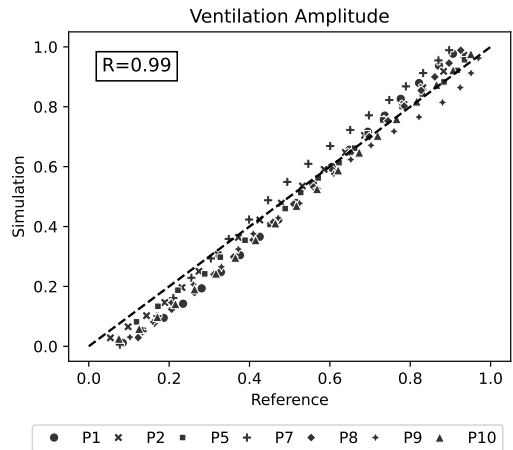


**Fig. 8:** Comparison of sum of pulmonary pixel intensities between simulated and reference EIT for multiple inflation states.

Having established that the absolute amount of aeration is correctly predicted across multiple ventilation states, we now turn our attention to establishing the accuracy of the model-predicted relative regional ventilation across the entire tidal

volume. To this end, we repeat our previous analysis regarding correlation of pulmonary pixel intensities from the preceding section. The obvious change is that this time this comparison is applied to the normalized representations  $\hat{Z}$ , and repeated across multiple inflation states corresponding to  $I = \{0.2, 0.4, 0.6, 0.8, 0.95\}$ .

$I =$	0.20	0.40	0.60	0.80	0.95
R ( $\emptyset$ )	0.81	0.81	0.82	0.83	0.82
RMSE ( $\emptyset$ )	0.15	0.15	0.15	0.14	0.15

**Table 2:** Average metrics  $R$  and RMSE for the regional ventilation across different ventilation states.

With the resulting metrics averaged over the population ensemble listed in Table 2, we observe that the model agreement remains largely unaffected and stable across all possible ventilation states comprising the full tidal range of mechanical ventilation.

## 4 Discussion

In this study, we have provided systematic validation of a reduced-dimensional computational lung models, comparing numerical predictions of the regional ventilation against measured clinical reference data for mechanically ventilated ARDS patients. Very good to excellent agreement between numerical predictions and reference clinical data was observed, even despite the pathophysiological inhomogeneities of the lungs and the known intrinsic limitations of the clinical data. In addition to demonstrating agreement of anteroposterior and lateral projections of the ventilation state close to the resolution limitations of EIT, our computational model also yielded predictions largely congruent with the reference data even when considering the *full* spatial resolution across the *entire* dynamic range of mechanical ventilation. Considering the complex nature of the clinical data as well as the required modeling assumptions underlying the electrodynamic simulation, it furthermore seems plausible that remaining observable discrepancies may at least partially be attributed to data limitations. Exemplary, the evident anteroposterior shift or rotation for patient 8 and 10 in Figure 7 might be explained by small inaccuracies in the modeling of the electrode placements in the electrodynamic simulation. Even for cases exhibiting the largest discrepancy between model predictions and clinical measurements, it seems plausible that the clinical information conveyed by model predictions concerning the lung is qualitatively very close to the measured EIT.

The computational lung model, therefore, provided correct predictions of the heterogeneous ventilation distribution and successfully accounted for the strong intra- and inter-patient variability of the pathophysiological lung state underlying ARDS. Limitations of the results presented largely coincide with the inherent limitations of EIT, notably (*i*) the restriction of the validation to a two-dimensional transverse plane, (*ii*) potential errors or bias introduced in the reconstruction, and (*iii*) measurement noise and epistemic uncertainty associated with the clinical data. To our knowledge, this is the first in-depth and quantitative validation study of patient-specific lung models that provide detailed, regional information about the ventilation and mechanical state of heterogeneously damaged parenchymal lung tissue during mechanical ventilation.

In addition, our simulation approach is embedded into a comprehensive computational framework that includes automated image processing, model generation, and calibration. In contrast to previous methodological proof-of-concept research [27, 35], which requires a lot of manual work and fine-tuning during model creation and simulation setup, we can create simulation-ready models from images in minutes and deliver final results and analysis within an hour. As a result, our approach is fast enough to be applied in a clinical setting.

At this point, we would like to stress that model predictions offer several important advantages over pulmonary monitoring using EIT. First, our model provides prediction for the state of the entire lung parenchyma, whereas EIT is limited to a single transverse plane, typically between the 4th and 5th intercostal space. Second, the model provides a much higher spatial resolution. Third, our modeling approach enables *in silico* investigations of counterfactual or hypothetical scenarios for arbitrary ventilator settings. Lastly, and perhaps most importantly, in contrast to EIT the computational model is not limited to provide information only on the regional ventilation. While functional EIT can also provide information on the strain of the lung parenchyma, it is inherently based on additional approximations and limited to the relative strain difference between end-inspiratory and end-expiratory state. In contrast, our model computes *absolute* mechanical quantities like stress, strain, or any quantity derived thereof (such as mechanical power or work), and thereby enabling - for the first time - a quantitative comparison between patients. With the only prerequisite for the model predictions being the CT scan and the ventilatory data, unlike EIT it is also not necessary to attach additional sensors to the patient.

## 5 Conclusion

In conclusion, having established the ability of the computational lung model to correctly resolve

the regional biomechanical behavior of the lung parenchyma during mechanical ventilation, this opens up the perspective to link model predictions with assumed pathways underlying ventilator-induced lung injury. By making use of highly resolved biomechanical models as employed in our work, one may introduce novel, model-based mechanical biomarkers to objectively quantify the overall regional ventilatory load for individual patients.

As indicated in Figure 9, this implies that one could use the computational model to *(i)* predict how different hypothetical ventilation settings affect the lung and its ventilation, *(ii)* compare the risk of injurious processes to the lung tissue and *(iii)* ultimately choose an optimal patient-specific lung protective ventilation strategy, which is deemed optimal according to predicted biomarkers.

Towards this goal, future work will involve the validation of model predictions against 4D-CT data, in contrast to EIT offering higher spatial resolution at the expense of decreased temporal resolution. Additionally, of course, there is ongoing research to extend the computational lung model and its validation towards more complex physical and physiological phenomena, such as exemplarily resolving recruitment and de-recruitment phenomena [36, 51].

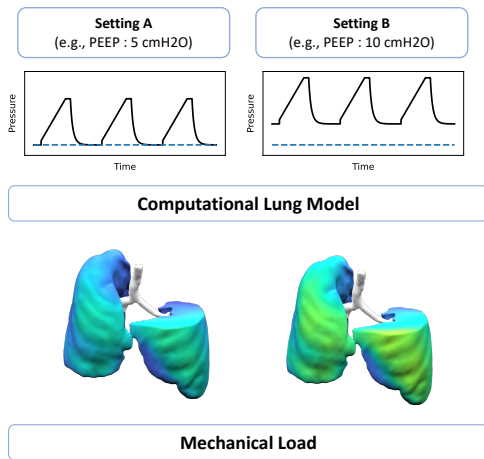


**Fig. 9:** The computational lung model enables predictions regarding multiple hypothetical choices of the ventilation settings, yielding exemplarily the spatially resolved cumulative mechanical load over time as a function of the chosen PEEP.

## Supplementary information (SI)

Supplementary information is provided in a separate document attached to this article.

## Funding

T.B., I.F., and W.A.W. gratefully acknowledge the financial support by the Deutsche Forschungsgemeinschaft (DFG, German Research Foundation) in the project BE6526/1-1—WA1521/26-1. W.A.W. and M.Lu. gratefully acknowledge the financial support by BREATHE, a Horizon 2020-ERC-2020-ADG project (101021526-BREATHE)

## Competing interests

J.B., K.R.W., K.W.M., and W.A.W. hold shares of Ebenbuild. All other authors declare no competing interests.

## Ethics approval and consent to participate

For this study, we analyzed data that was collected within the scope of the SMART-Study (DRKS-ID: DRKS00017151). The study was approved by the Ethics Committee of the Medical Faculty of the Christian-Albrechts-Universität Kiel (Ethics Committee Number D 485/17) and carried out in accordance with the Helsinki Declaration. Written informed consent was obtained from all patients or their legal representatives.

## Consent for publication

Not applicable.

## Availability of data and materials

All the data described and generated in the paper and SI is available upon reasonable request from the corresponding author. Our source code for the electrodynamic simulation and the EIT reconstruction based on EIDORS is available online at <https://gitlab.com/xenotaph3/holeshed> under the BSD-3 clause license. The biomechanical simulations described in this paper were created using our own in-house codebase. Unfortunately, the source code underlying the model generation and biomechanical simulation constitutes a proprietary asset which we are unable to share at the current time.

## Authors' contributions

T.B., J.B., I.F., D.S., K.W.M., and W.A.W. conceptualized and designed the research. T.B. planned and conducted the clinical study to collect the data. T.B., I.F., M.L., M.Lu., and A.S. collected and analyzed the clinical data. M.R. performed the simulation setup and runs. M.R., M.Lu., and K.R.W. contributed to software development and model setup. M.R., K.R.W., M.C.W., M.Lu., and J.B.

did post-processing, data analysis, and visualization of simulation results. M.R. and J.B. wrote the manuscript. All authors reviewed the manuscript.

## Acknowledgements

Not applicable.

## Abbreviations

<b>ARDS</b>	Acute Respiratory Distress Syndrome
<b>AU</b>	Arbitrary Units
<b>CT</b>	Computed Tomography
<b>EIT</b>	Electrical Impedance Tomography
<b>GREIT</b>	Graz Consensus Reconstruction Algorithm for EIT
<b>PEEP</b>	Positive End Expiratory Pressure
<b>RMSE</b>	Root Mean Square Error
<b>VILI</b>	Ventilator-Induced Lung Injury

# A Supplementary Information

## Computational Lung Model

The following provides a short introduction to the computational lung model, which has been developed over the last two decades and published in a number of peer-reviewed papers (as cited in the main text). It is intended as a service for the reader and strives to convey the basic concepts, without requiring detailed prior knowledge in the domain of computational physics and numerical modeling.

Before we delve deeper into how the model is constructed, let us briefly consider the physiological features and processes that the computational lung model has to resolve during the course of mechanical ventilation: for positive pressure ventilation, a driving pressure at the trachea leads to a non-zero transpulmonary pressure affecting the distension and inflation of the lung parenchyma with corresponding airflow and tidal volume. Starting from the endotracheal tube during the inspiratory phase, air traverses in initially relatively turbulent flow down the larger airway structures and disperses into the lung parenchyma by following sequences of ever smaller self-similar asymmetric branching structures. After 16 to 24 generations of conductive airways, the airflow reaches the respiratory zone, with the air finally dispersing into respiratory bronchioli, then alveolar sacs, finally reaching roughly 480 million individual alveoli. For the pathological lung parenchyma, this delicate and complex structure loses its relative homogeneity, with mechanical properties as well as resulting inflation and deflation cycles becoming increasingly heterogeneous in nature [52]. Thereby, the already existing intrinsic intra-patient variability between healthy individuals (e.g., lung volume) increases further due to local pathophysiological variability introduced by ARDS, such as —exemplarily— inflammatory processes [7] leading to consolidations or compression atelectasis in dependent regions. The challenging situation faced by clinicians then lies in the complex manner in which the pathophysiological state of the lung parenchyma interacts with the forces exerted by the mechanical ventilator. The resulting strain, stress, and overall trauma strongly depend on the *specific* forcing pressure and flow applied at the trachea, which is determined by the clinicians choice of ventilator settings [53, 54]. In order to predict and numerically capture the biomechanical behavior of the lung, it is therefore necessary to identify a model that can resolve the fundamental underlying physical phenomena subject to the particular physiological and pathophysiological state.

## Patient-specific Model Construction

To accomplish the goal of a *patient-specific* model, the first step of model construction leverages machine learning and computer vision approaches to automatically segment and identify relevant physiological features from a thorax CT<sup>3</sup>. This step yields information on the exact shape, volume, and boundaries of the lungs, their subdivision into lobes along fissure lines, as well as the airway tree extending from the trachea, as shown in Figure 3. When reaching the resolution limit of the CT scan, the segmented airways are further extended by a space-filling airway tree growth algorithm [55] that continues the dyadic and self-similar branching structure within each lobe according to known statistical and morphological properties [56], yielding exemplarily the airway tree depicted in Figure 3. The use of these hybrid patient-specific/morphometric airway trees is based on the premise that beyond a certain structural size, it is no longer the specific geometry of individual airways that matter but rather the morphological properties of the airway tree. The generational depth at which one truncates the growth of the artificial airway tree can be seen as a measure of model complexity - we consider up to 16 generations, reaching the threshold of the respiratory airways. Beyond the terminal airways, the model does no longer consider individual structures in terms of airways or alveoli, and instead introduces models introducing an aggregate description of the compound behavior of bronchioli, alveolar sacs and alveoli - this can be regarded as lumped descriptions of the *local* behavior of the respiratory zone. For both airways as well as the respiratory zone the formulation we employ introduces reduced-dimensional models that characterize salient behavior at significantly reduced numerical cost, as will be further detailed in the ensuing subsections. In the following, we provide a brief *conceptual* introduction, discussing the reduced-dimensional elements for airways and lung parenchyma, which serve as model primitives and - once globally coupled - capture the behavior of the entire respiratory system.

## Conducting Airways

In the simplest case, an individual airway segmented from the CT scan can be considered as an elongated tubular structure of a certain length  $l_{aw}$  and radius  $r_{aw}$  through which laminar, incompressible, and rotationally symmetric flow  $Q$  occurs purely as a function of the forcing pressure differential  $\Delta p$  as well as the resistance to the flow offered by the airway. This can be expressed as

<sup>3</sup>Additional manual inspection and correction were performed for the validation cases, since the focus lies on assessing the model predictions

$$Q = \frac{\pi \cdot r_{aw}^4}{8 \cdot \eta \cdot l_{aw}} \cdot \Delta p \quad , \quad (\text{A1})$$

with  $\eta$  the dynamic viscosity of the fluid (Poiseuille flow). In essence, this simplifies a complex three-dimensional fluid-structure interaction dependent on patient-specific geometrical features ( $l_{aw}, r_{aw}$ ) into a highly simplified description. This is what - in abstract terms - we refer to an *airway element* of the model. Adding increased complexity in the physical model of an airway element (compressibility of air, turbulence, non-rigid airways) will lead to increased complexity of the mathematical model defined by Eq. (A1), but the conceptual idea remains unchanged. Since we also know for each branching point of the airway tree that mass and momentum must be conserved, descriptions of individual airway elements can be coupled and assembled into a global system, implying that one can jointly determine time-dependent pressure and flow over the entire airway tree (see Figure A1). Once the flow of air has traversed through the maximum number of resolvable airway generations (up to 16), we model the local behavior of the lung parenchyma in the surrounding area of each terminal airway.

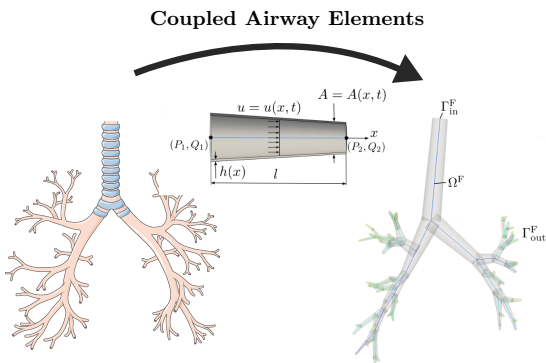


**Fig. A1:** The airway tree is reduced to coupled 0D airway elements, derived from the Navier-Stokes equation under simplifying assumptions. Illustration adapted from [57], and making use of Servier Medical Art (under Creative Commons Attribution 3.0).

### Alveolar Clusters

The lung parenchyma beyond the conducting airways - comprised of respiratory bronchioli and alveoli - is modeled by alveolar clusters that capture the *locally* homogenized behavior of a small sub-region of the lung parenchyma. The name of this substitute model element - alveolar cluster - derives from it capturing the aggregate behavior of a local *cluster* of several thousands or tens of thousands of alveoli. Intuitively explained, alveolar clusters

define local exit-compartment models attached to terminal airways coupled via flow and pressure. It acts as a substitute model for a local ensemble of small-scale respiratory bronchioli and alveoli in the vicinity of the terminal airway, emulating the local behavior of the lung parenchyma, complying and/or counteracting the airflow through terminal airways through various static, dynamic, and viscous effects.

In Figure (A2), a simple example for such a reduced-dimensional alveolar cluster element at the distal end of the conducting airway tree is given, with the schematic representation relating various physical phenomena to mechanically equivalent behavior, i.e., springs or dampening elements, counteracting the inflow (or outflow) of air  $Q$ . The forcing pressure differential experienced by each alveolar cluster corresponds to the transpulmonary pressure and arises as the pressure differential between alveolar and pleural pressure  $p_{pl}$ . More for-

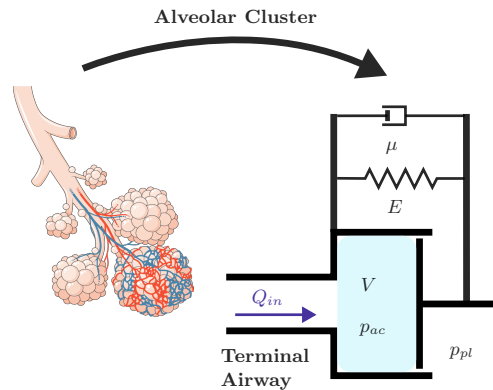


**Fig. A2:** The respiratory zone of the lung parenchyma, comprised of bronchioli and alveoli, is modeled as alveolar clusters, acting as an exit compartment for the terminal airways. Mechanically equivalent behavior can be expressed in terms of simple elements such as, e.g., springs and dampeners. Illustration makes use of Servier Medical Art under Creative Commons Attribution 3.0).

mally, the alveolar clusters capture the local behavior of the lung parenchyma through a viscoelastic model relating strain and stress within the lung tissue [40–43, 58, 59]. Similarly to the discussion for airways, increasingly complex phenomena giving rise to increasingly complex rheological behavior can be modeled by expanding upon the prototypical spring and damper elements depicted in A2.

Numerical discretization of the coupled alveolar cluster and airway descriptions yields a differential algebraic system of equations, which we solve iteratively by making use of suitable time-integration methods [60] — i.e., we simulate the state of the lung parenchyma over time, as a function of time-varying pressure or flow applied by the mechanical ventilator (depending on the ventilator mode). In

contrast to a simplistic one-compartment model, which has exactly one flow rate, one volume, and one pressure, depending on the chosen generational depth of the airway tree, the model comprises  $10^4$  to  $10^6$  degrees of freedom, corresponding to time-dependent and spatially resolved flow, volume, pressure, strain and stress distributed over the entire lung parenchyma.

### Pleurae, chest wall, and diaphragm

An aspect not discussed in detail so far is that the behavior of the lung parenchyma during mechanical ventilation of course also depends on the surrounding pleural pressure. The pleural pressure and its variability are defined by several aspects [61], such as the compliance of the thoracic cage counteracting volumetric changes of the lung, sternocostal articulation, pleural interface, and intra-abdominal pressure. In addition, hydrostatic pressure increases towards dependent regions conditional on gravity and patient positioning (e.g., prone, supine), and of course, any spontaneous breathing efforts by the patient result in muscular activity modulating the pleural pressure.

While the patients enrolled in the study were sufficiently sedated to disregard inspiratory efforts as a meaningful contributor to pleural pressure variations, gravitational forces as well as elastic recoil of the chest wall are accounted for by means of a suitable external pressure boundary condition acting on the alveolar clusters. Pertinent patient-specific parameters relating to the chest-wall are identified and isolated during the calibration process using esophageal pressure measurements, as will be discussed in further detail. The pleural pressure boundary condition also encompasses a hydrostatic pressure component that depends on the known positioning of the patient and on the weight of the lungs as determined from the CT image, performing a density and volume analysis to account for the spatial variability of the pleural pressure.

### Model Calibration

While the model matches the patient-specific anatomy of the patient by being constructed on the basis of a CT scan, further adaptations are required to capture the specific (patho)-physiology of each patient. We combine a two step optimization approach with our model and to this end incorporate both information from the CT scan, as well as additional time series data from the mechanical ventilator. The time series data comprises ventilation pressure, flow and esophageal pressure, containing information about the *global* characteristics of the respiratory system, e.g., the global respiratory system compliance  $C_{rs}$ , or the overall impact of viscous dampening effects. In contrast, the Hounsfield attenuation values from the CT provide regional

information, for instance, insight about the reduction of local lung volume as a function of pathophysiological changes. As a consequence of this, alveolar clusters resolving a strongly consolidated subregion of the lung parenchyma will exemplarily exhibit significantly decreased compliance.

In the first step, we use a suitable optimization algorithm to identify global behavior which minimizes the misfit for observed tracheal flow and esophageal pressure, while providing the additional constraint that the model predicted pleural pressure must also be in agreement with known physiological values at functional residual capacity [62]. This constitutes a continued development from prior work relying on static fitting, offering a higher degree of accuracy while simultaneously posing less stringent requirements with regards to the available ventilatory patient data. With the global behavior of the respiratory system calibrated, the second step involves a further resolution of the global behavior towards regional adjustment of mechanical properties of sub-regions of the lung parenchyma (i.e., modulating behavior of individual alveolar clusters on the basis of Hounsfield attenuation values). By adjusting parameters of individual alveolar clusters relating to constitutive and volumetric properties, we account for heterogeneous - i.e. spatially varying - pathophysiological changes induced by ARDS.

### Electrical Impedance Tomography

In order to employ electrical impedance tomography for pulmonary monitoring during mechanical ventilation [63, 64], an electrode belt is positioned around the thorax of each patient, with electrical stimulations - i.e., driving current - being injected at high temporal resolution according to predefined and quickly alternating stimulation patterns. Since the spatially variable conductivity of the lung parenchyma depends on its aeration, the resulting potential field and the corresponding measured complex-valued voltage signals at the electrode belt are necessarily not only a function of the intrathoracic structure, but also depend on the regional ventilation distribution within the lung. By quickly cycling through stimulation patterns and measuring the potential field at the remaining receiving electrodes, time-dependent information can be aggregated on the regional ventilation of the lung. Using a 32-electrode belt attached to an Elisa 800 ventilator with integrated EIT, at each time-step voltage data  $v \in \mathbb{C}^{1024}$  is obtained at a sampling rate of 50 Hz (the dimensionality is defined by the number of electrodes as well as stimulation and measurement patterns).

While there are certain practical complexities, measuring this clinical voltage data corresponds to well-established clinical processes already widely in use on ICUs during mechanical ventilation. The

subsequent reconstruction of the regional ventilation from the voltage data defines an *inverse* problem, and - similarly to the discussion of the electrodynamic simulation (2.3) - is predicated upon the existence of a forward model, which essentially relates measured voltages with injected stimulation patterns and the conductivity of the lung parenchyma.

### Forward Problem

The behavior of electrodynamic fields propagating across the torso is known to be characterized by Maxwell’s equations, which for our purposes - under several simplifying assumptions - can be reduced to a single, scalar elliptic partial differential equation on the domain of the patient’s torso, i.e. for all  $x \in \Omega_{torso}$

$$\operatorname{div}(\sigma(x) \cdot \nabla \Phi(x)) = 0 \quad (\text{A2})$$

we relate the tissue conductivity  $\sigma(x)$  and the resulting potential field  $\Phi(x)$ . For the sake of our discussion it is not relevant to examine the specific structure of this equation, nor the specifics of the boundary conditions which have been omitted from explicit representation. Instead we simply observe that both the conductivity  $\sigma(x)$  and the potential field  $\Phi(x)$  resulting from the currents injected at the electrodes spatially vary over the torso, and that their interdependence is defined by fundamental physical laws mathematically expressed by Eq. (A2). Using well-established numerical discretization techniques such as Finite Elements [65] this equation can be solved to obtain resulting simulated voltage, i.e., one computes the potential field across the torso conditional on the conductivity field and the stimulating currents applied at the electrodes (*forward problem*). In order to solve the forward problem we again rely on EIDORS [46], which is also employed for the solution of the inverse problem using GREIT (*Graz consensus Reconstruction algorithm for EIT*).

### Inverse Problem

The fundamental goal of electrical impedance tomography is however to traverse the *inverse* route, i.e., to identify the conductivity field  $\sigma(x)$  over the lung parenchyma which can adequately explain a set of observed voltage measurements. This conceptually implies to minimize the misfit or maximize the likelihood of model predictions with regards to observed voltage data, generally subject to additional prior information or additional regularization (*inverse problem*). For pulmonary monitoring via EIT, we follow the established and generally more stable approach of *difference* EIT, where regional ventilation is inferred on the basis

of *perturbations* of the voltage data from an end-expiratory reference state. This behaves favorable, because unknown but constant obfuscators - such as the intrathoracic structure and variations of contact impedances of electrodes - do not enter directly into the reconstruction problem. As previously mentioned, for the reconstruction we employ GREIT [45], as it is a well-established and widely used algorithm with an available open-source implementation [46]. The outcome of the reconstruction is generally a two-dimensional regional ventilation map varying over time, which may be represented as a two-dimensional  $Z$ , resolving the regional ventilation across a transverse cut-slice of the patient’s thorax between the 4th and 5th intercostal space (see Figure 2 and ventilation maps in Figure 1). As such, GREIT maps voltage data to two-dimensional intensity images. For the resolution we employ for our validation purposes,  $Z$  is given by a  $64 \times 64$  grid of pixels, which we may represent as  $Z \in \mathbb{R}^{64 \times 64}$ . Mathematically, this is a square matrix comprised of real-valued numbers. GREIT therefore defines a mapping  $\mathbb{C}^{1024} \mapsto \mathbb{R}^{64 \times 64}$ , with voltage measurements  $v$  giving rise to the EIT image  $Z$ . In this EIT image, pixel intensity relates to an increase of inverse conductivity, and thus a larger degree of local aeration of the lung parenchyma. For a more in-depth discussion of EIT for respiratory monitoring as well as the specifics of the inverse problem setting we refer the reader - due to the inherent scope and complexity - to the appropriate literature for further information [63, 66, 67]. For our purposes, we simply conclude that conditional on voltage data (be it simulated or measured) the inversion underlying EIT yields an image  $Z$  carrying information on the local aeration and regional ventilation of the lung across a two-dimensional transverse plane. By conducting the identical inverse reconstruction approach both for measured clinical voltage data as well as for simulated voltage data resulting from the computational lung model, we can compare predictions of regional ventilation against reference data. While the computational lung model permits predictions beyond merely regional ventilation (such as e.g. local strain), the validation centers around the regional ventilation because it is the only primary information than can be derived directly from EIT without necessitating further assumptions and approximations.

### Technical Details

We close this section with some technical details that warrant explicit mention. First, patient-specific torso meshes used for the generation of simulated voltages are also used for the solution of the inverse problem underlying EIT, enabling reconstructions with a higher degree of fidelity compared to population-averaged torso geometries generally in use for bedside EIT [48].

Secondly, in the context of the validation effort it has to be observed that the employed reconstruction algorithm follows a heuristic approach and has several non-uniquely defined parameters that inevitably arise due to the necessity to regularize the ill-conditioned inverse problem arising from Eq. (A2), thereby implicitly affecting the results. There does not exist an established generic manner of setting these parameters, as they are generally highly problem-dependent and will vary as a function of the specific characteristics of the measured clinical data (e.g, number and placement of electrodes, electrical and movement noise level, improper and detached electrodes). In absence of definitive 4D-CT data, we have followed the most commonly employed approach of determining reconstruction parameters on the basis of qualitative assessment of reconstructions, with identical reconstruction parameters used across the entire patient cohort. Likewise, reconstruction parameters of GREIT are chosen identical for both simulated as well as measured voltages with exception of a small discrepancy in the noise figure, due to the lack of noise affecting the simulated data.

## References

- [1] Serpa Neto, A. *et al.* Mechanical power of ventilation is associated with mortality in critically ill patients: An analysis of patients in two observational cohorts. *Intensive Care Medicine* **44**, 1914–1922 (2018).
- [2] Silva, P. L., Ball, L., Rocco, P. R. M. & Pelosi, P. Power to mechanical power to minimize ventilator-induced lung injury? *Intensive Care Medicine Experimental* **7**, 38 (2019).
- [3] Bates, J. H. T. & Smith, B. J. Ventilator-induced lung injury and lung mechanics. *Annals of Translational Medicine* **6**, 378–378 (2018).
- [4] Gattinoni, L., Protti, A., Caironi, P. & Carlesso, E. Ventilator-induced lung injury: The anatomical and physiological framework. *Critical Care Medicine* **38**, S539–548 (2010).
- [5] Gattinoni, L., Collino, F. & Camporota, L. Ventilator induced lung injury: A case for a larger umbrella? *Intensive Care Medicine* **50**, 275–278 (2024).
- [6] Mead, J., Takishima, T. & Leith, D. Stress distribution in lungs: A model of pulmonary elasticity. *Journal of Applied Physiology* **28**, 596–608 (1970).
- [7] González-López, A. *et al.* Lung strain and biological response in mechanically ventilated patients. *Intensive Care Medicine* **38**, 240–247 (2012).
- [8] Dreyfuss, D. & Hubmayr, R. What the concept of VILI has taught us about ARDS management. *Intensive Care Medicine* **42**, 811–813 (2016).
- [9] Marini, J. J. Evolving concepts for safer ventilation. *Critical Care* **23**, 114 (2019).
- [10] Grasselli, G. *et al.* ESICM guidelines on acute respiratory distress syndrome: Definition, phenotyping and respiratory support strategies. *Intensive Care Medicine* **49**, 727–759 (2023).
- [11] Putensen, C., Theuerkauf, N., Zinserling, J., Wrigge, H. & Pelosi, P. Meta-analysis: Ventilation strategies and outcomes of the acute respiratory distress syndrome and acute lung injury. *Annals of Internal Medicine* **151**, 566–576 (2009).
- [12] Kollisch-Singule, M. C. *et al.* Looking beyond macroventilatory parameters and rethinking ventilator-induced lung injury. *Journal of Applied Physiology (Bethesda, Md.: 1985)* **124**, 1214–1218 (2018).
- [13] Khan, Y. A., Fan, E. & Ferguson, N. D. Precision Medicine and Heterogeneity of Treatment Effect in Therapies for ARDS. *Chest* **160**, 1729–1738 (2021).
- [14] Chen, H. *et al.* Lung morphology impacts the association between ventilatory variables and mortality in patients with acute respiratory distress syndrome. *Critical Care* **27**, 59 (2023).
- [15] Juschten, J. *et al.* Between-trial heterogeneity in ARDS research. *Intensive Care Medicine* **47**, 422–434 (2021).
- [16] Villar, J., Blanco, J. & Kacmarek, R. M. Current incidence and outcome of the acute respiratory distress syndrome. *Current Opinion in Critical Care* **22**, 1–6 (2016).
- [17] Sadana, D. *et al.* Mortality associated with acute respiratory distress syndrome, 2009–2019: A systematic review and meta-analysis. *Critical Care and Resuscitation* **24**, 341–351 (2022).
- [18] Gomez-Laberge, C., Arnold, J. H. & Wolf, G. K. A Unified Approach for EIT Imaging of Regional Overdistension and Atelectasis in Acute Lung Injury. *IEEE Transactions on Medical Imaging* **31**, 834–842 (2012).
- [19] Calfee, C. S. *et al.* Subphenotypes in acute respiratory distress syndrome: Latent class analysis of data from two randomised controlled trials. *The Lancet Respiratory Medicine* **2**, 611–620 (2014).
- [20] Calfee, C. S. *et al.* Acute respiratory distress syndrome subphenotypes and differential response to simvastatin: Secondary analysis of a randomised controlled trial. *The Lancet Respiratory Medicine* **6**, 691–698 (2018).
- [21] Heijnen, N. F. L. *et al.* Biological Subphenotypes of Acute Respiratory Distress Syndrome Show Prognostic Enrichment in Mechanically Ventilated Patients without Acute Respiratory Distress Syndrome. *American journal of respiratory and critical care medicine* **203**, 1503–1511 (2021).
- [22] Maddali, M. V. *et al.* Validation and utility of ARDS subphenotypes identified by machine-learning models using clinical data: An observational, multicohort, retrospective analysis. *The Lancet. Respiratory medicine* **10**, 367–377 (2022).
- [23] Gattinoni, L. *et al.* The future of mechanical ventilation: Lessons from the present and the

- past. *Critical Care* **21**, 183 (2017).
- [24] Beitler, J. R. *et al.* Advancing precision medicine for acute respiratory distress syndrome. *The Lancet Respiratory Medicine* **10**, 107–120 (2022).
- [25] Peine, A. *et al.* Development and validation of a reinforcement learning algorithm to dynamically optimize mechanical ventilation in critical care. *npj Digital Medicine* **4**, 32 (2021).
- [26] Kondrup, F. *et al.* Towards Safe Mechanical Ventilation Treatment Using Deep Offline Reinforcement Learning. *Proceedings of the AAAI Conference on Artificial Intelligence* **37**, 15696–15702 (2023).
- [27] Roth, C. J., Yoshihara, L., Ismail, M. & Wall, W. A. Computational modelling of the respiratory system: Discussion of coupled modelling approaches and two recent extensions. *Computer Methods in Applied Mechanics and Engineering* **314**, 473–493 (2017).
- [28] Roth, C. J., Yoshihara, L. & Wall, W. A. in *Computational Modeling of Respiratory Biomechanics* (ed. Narayan, R.) *Encyclopedia of Biomedical Engineering* 70–80 (Elsevier, 2019).
- [29] Neelakantan, S. *et al.* Computational lung modelling in respiratory medicine. *Journal of The Royal Society Interface* **19**, 20220062 (2022).
- [30] Mellenthin, M. M. *et al.* Using injury cost functions from a predictive single-compartment model to assess the severity of mechanical ventilator-induced lung injuries. *Journal of Applied Physiology* **127**, 58–70 (2019).
- [31] Rees, S. E. & Karbing, D. S. Determining the appropriate model complexity for patient-specific advice on mechanical ventilation. *Biomedical Engineering / Biomedizinische Technik* **62** (2017).
- [32] Sundaresan, A., Yuta, T., Hann, C. E., Geoffrey Chase, J. & Shaw, G. M. A minimal model of lung mechanics and model-based markers for optimizing ventilator treatment in ARDS patients. *Computer Methods and Programs in Biomedicine* **95**, 166–180 (2009).
- [33] Morton, S. *et al.* A virtual patient model for mechanical ventilation. *Computer Methods and Programs in Biomedicine* **165**, 77–87 (2018).
- [34] Ismail, M., Comerford, A. & Wall, W. A. Coupled and reduced dimensional modeling of respiratory mechanics during spontaneous breathing. *International Journal for Numerical Methods in Biomedical Engineering* **29**, 1285–1305 (2013).
- [35] Roth, C. J., Becher, T., Frerichs, I., Weiler, N. & Wall, W. A. Coupling of EIT with computational lung modeling for predicting patient-specific ventilatory responses. *Journal of Applied Physiology* **122**, 855–867 (2017).
- [36] Geitner, C. M. *et al.* Pressure- and time-dependent alveolar recruitment/derecruitment in a spatially resolved patient-specific computational model for injured human lungs. *International journal for numerical methods in biomedical engineering* **40**, e3787 (2024).
- [37] Grill, M. J. *et al.* In silico high-resolution whole lung model to predict the locally delivered dose of inhaled drugs (2023). [2307.04757](https://doi.org/10.2307/04757).
- [38] ARDS Definition Task Force *et al.* Acute respiratory distress syndrome: The Berlin Definition. *JAMA* **307**, 2526–2533 (2012).
- [39] Roth, C. J., Ismail, M., Yoshihara, L. & Wall, W. A. A comprehensive computational human lung model incorporating inter-acinar dependencies: Application to spontaneous breathing and mechanical ventilation. *International Journal for Numerical Methods in Biomedical Engineering* **33**, e02787 (2017).
- [40] Birzle, A. M., Martin, C., Yoshihara, L., Uhlig, S. & Wall, W. A. Experimental characterization and model identification of the nonlinear compressible material behavior of lung parenchyma. *Journal of the Mechanical Behavior of Biomedical Materials* **77**, 754–763 (2018).
- [41] Birzle, A. M., Hobrack, S. M. K., Martin, C., Uhlig, S. & Wall, W. A. Constituent-specific material behavior of soft biological tissue: Experimental quantification and numerical identification for lung parenchyma. *Biomechanics and Modeling in Mechanobiology* **18**, 1383–1400 (2019).
- [42] Birzle, A. M. & Wall, W. A. A viscoelastic nonlinear compressible material model of lung parenchyma – Experiments and numerical identification. *Journal of the Mechanical Behavior of Biomedical Materials* **94**, 164–175 (2019).
- [43] Birzle, A. M., Martin, C., Uhlig, S. & Wall, W. A. A coupled approach for identification of nonlinear and compressible material models for soft tissue based on different experimental setups - Exemplified and detailed for

- lung parenchyma. *Journal of the Mechanical Behavior of Biomedical Materials* **94**, 126–143 (2019).
- [44] Roth, C. J. *et al.* Correlation between alveolar ventilation and electrical properties of lung parenchyma. *Physiological Measurement* **36**, 1211–1226 (2015).
- [45] Adler, A. *et al.* GREIT: A unified approach to 2D linear EIT reconstruction of lung images. *Physiological Measurement* **30**, S35–S55 (2009).
- [46] Adler, A. & Lionheart, W. R. B. Anonymous (ed.) *EIDORS: Towards a community-based extensible software base for EIT*. (ed. Anonymous) *Proceedings of the 6th Conference on Biomedical Applications of Electrical Impedance Tomography, London* (2005).
- [47] Dörfler, W. *et al.* in *What Is an Inverse and Ill-Posed Problem?* (eds Dörfler, W. *et al.*) *Wave Phenomena: Mathematical Analysis and Numerical Approximation* 281–284 (Springer International Publishing, Cham, 2023).
- [48] Thürk, F. *et al.* Effects of individualized electrical impedance tomography and image reconstruction settings upon the assessment of regional ventilation distribution: Comparison to 4-dimensional computed tomography in a porcine model. *PLOS ONE* **12**, e0182215 (2017).
- [49] Leonhardt, S. & Lachmann, B. Electrical impedance tomography: The holy grail of ventilation and perfusion monitoring? *Intensive Care Medicine* **38**, 1917–1929 (2012).
- [50] Hinz, J. *et al.* Regional Ventilation by Electrical Impedance Tomography: a comparison with ventilation scintigraphy in pigs. *Chest* **124**, 314–322 (2003).
- [51] Geitner, C. M. *et al.* An approach to study recruitment/derecruitment dynamics in a patient-specific computational model of an injured human lung. *International Journal for Numerical Methods in Biomedical Engineering* **39**, e3745 (2023).
- [52] Gattinoni, L., Tonetti, T. & Quintel, M. Regional physiology of ARDS. *Critical Care* **21**, 312 (2017).
- [53] Crooke, P. S., Gattinoni, L., Michalik, M. & Marini, J. J. Intracycle power distribution in a heterogeneous multi-compartmental mathematical model: Possible links to strain and VILI. *Intensive Care Medicine Experimental* **10**, 21 (2022).
- [54] Marini, J. J. & Rocco, P. R. M. Which component of mechanical power is most important in causing VILI? *Critical Care* **24**, 39 (2020).
- [55] Tawhai, M. H., Pullan, A. J. & Hunter, P. J. Generation of an anatomically based three-dimensional model of the conducting airways. *Annals of Biomedical Engineering* **28**, 793–802 (2000).
- [56] Weibel, E. R. *Morphometry of the Human Lung* (Springer-Verlag, Berlin Heidelberg, 1963).
- [57] Roth, C. J. Multi-dimensional Coupled Computational Modeling in Respiratory Biomechanics 230 (2017).
- [58] Modesto i Alapont, V., Aguar Carrascosa, M. & Medina Villanueva, A. Clinical implications of the rheological theory in the prevention of ventilator-induced lung injury. Is mechanical power the solution? *Medicina Intensiva (English Edition)* **43**, 373–381 (2019).
- [59] Guérin, C. *et al.* Regional lung viscoelastic properties in supine and prone position in a porcine model of acute respiratory distress syndrome. *Journal of Applied Physiology* **131**, 15–25 (2021).
- [60] Kunkel, P. *Differential-Algebraic Equations: Analysis and Numerical Solution* (European Mathematical Society, 2006).
- [61] Silva, P. L. & Gama de Abreu, M. Regional distribution of transpulmonary pressure. *Annals of Translational Medicine* **6**, 385 (2018).
- [62] Zielinska-Krawczyk, M., Krenke, R., Grabczak, E. M. & Light, R. W. Pleural manometry—historical background, rationale for use and methods of measurement. *Respiratory Medicine* **136**, 21–28 (2018).
- [63] Bachmann, M. C. *et al.* Electrical impedance tomography in acute respiratory distress syndrome. *Critical Care* **22**, 263 (2018).
- [64] Tomicic, V. & Cornejo, R. Lung monitoring with electrical impedance tomography: Technical considerations and clinical applications. *Journal of Thoracic Disease* **11**, 3122–3135 (2019).
- [65] Woo, E. J., Hua, P., Webster, J. G. & Tompkins, W. J. Finite-element method in electrical impedance tomography. *Medical & Biological Engineering & Computing* **32**, 530–536 (1994).

- [66] Frerichs, I. *et al.* Chest electrical impedance tomography examination, data analysis, terminology, clinical use and recommendations: Consensus statement of the TRanslational EIT developmeNt stuDy group. *Thorax* **72**, 83–93 (2017).
- [67] Adler, A. & Holder, D. *Electrical Impedance Tomography: Methods, History and Applications* (CRC Press, 2021).